Electronic supplementary information († ESI)
for
The emergence of bifunctional catalytic property by the introduction of Bi^{3+} in defect fluorite structured $PrO_{1.833}$

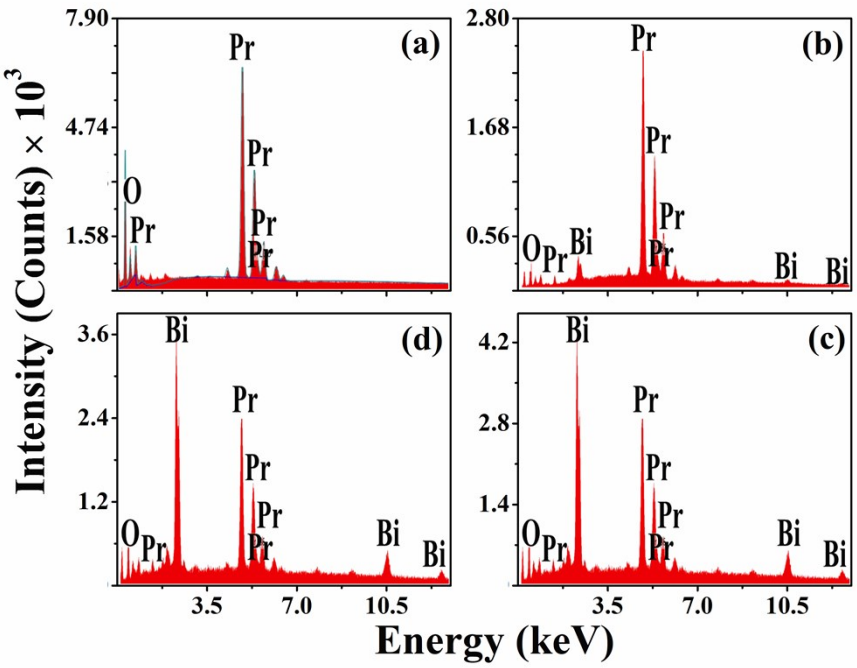

Fig. S1 shows the energy dispersive spectrum (EDS) along with the elemental analysis of (a) $PrO_{1.833}$, (b) $Pr_{0.90}Bi_{0.10}O_{2-\delta}$, (c) $Pr_{0.80}Bi_{0.20}O_{2-\delta}$ and (d) $Pr_{0.70}Bi_{0.30}O_{2-\delta}$ samples.

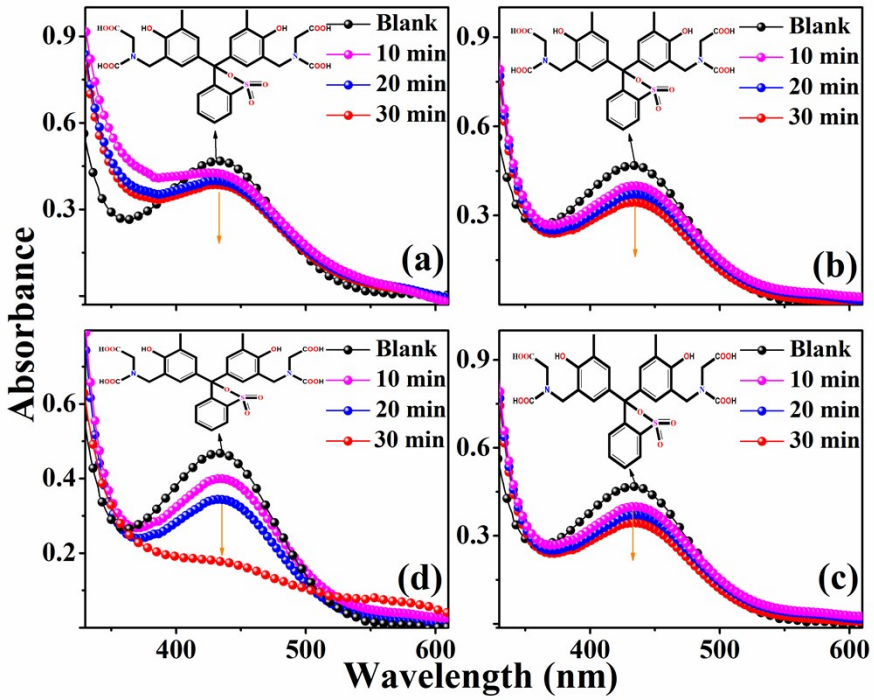

Fig. S2 shows time-dependent UV-visible spectra of XO (1×10^{-4} M) dye solution in the presence H_2O_2 and 20 mg of (a) $PrO_{1.833}$, (b) $Pr_{0.90}Bi_{0.10}O_{2-\delta}$, (c) $Pr_{0.80}Bi_{0.20}O_{2-\delta}$, and (d) $Pr_{0.70}Bi_{0.30}O_{2-\delta}$ sample.

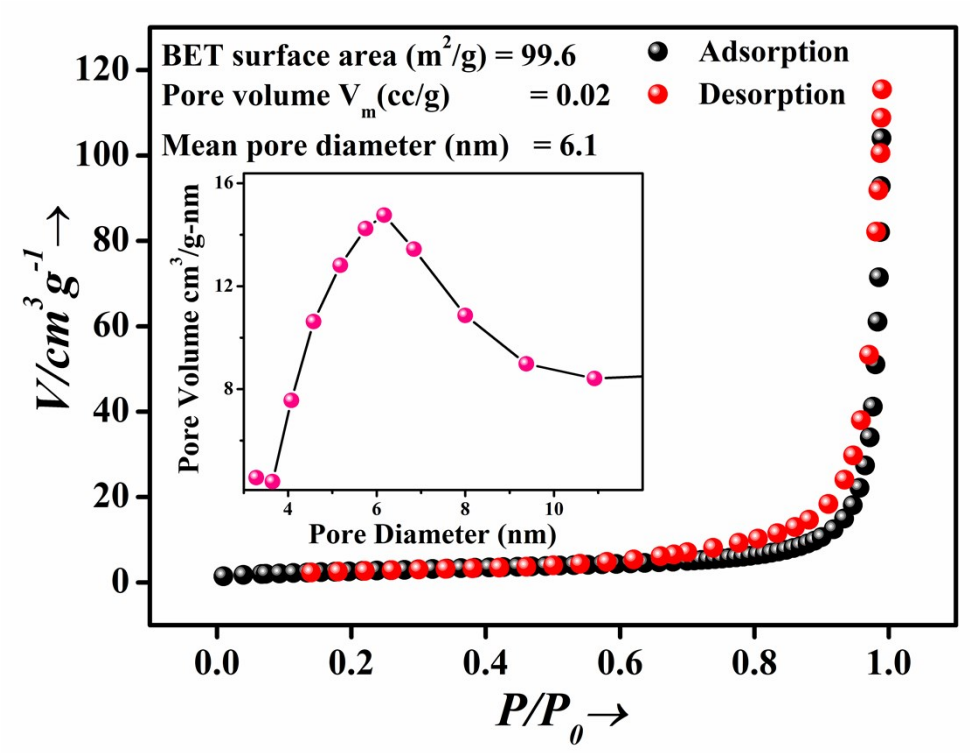

Fig. S3 shows nitrogen gas adsorption and desorption isotherms on the $Pr_{0.60}Bi_{0.40}O_{2-\delta}$ sample. The inset shows the plot of pore volume versus pore diameter.

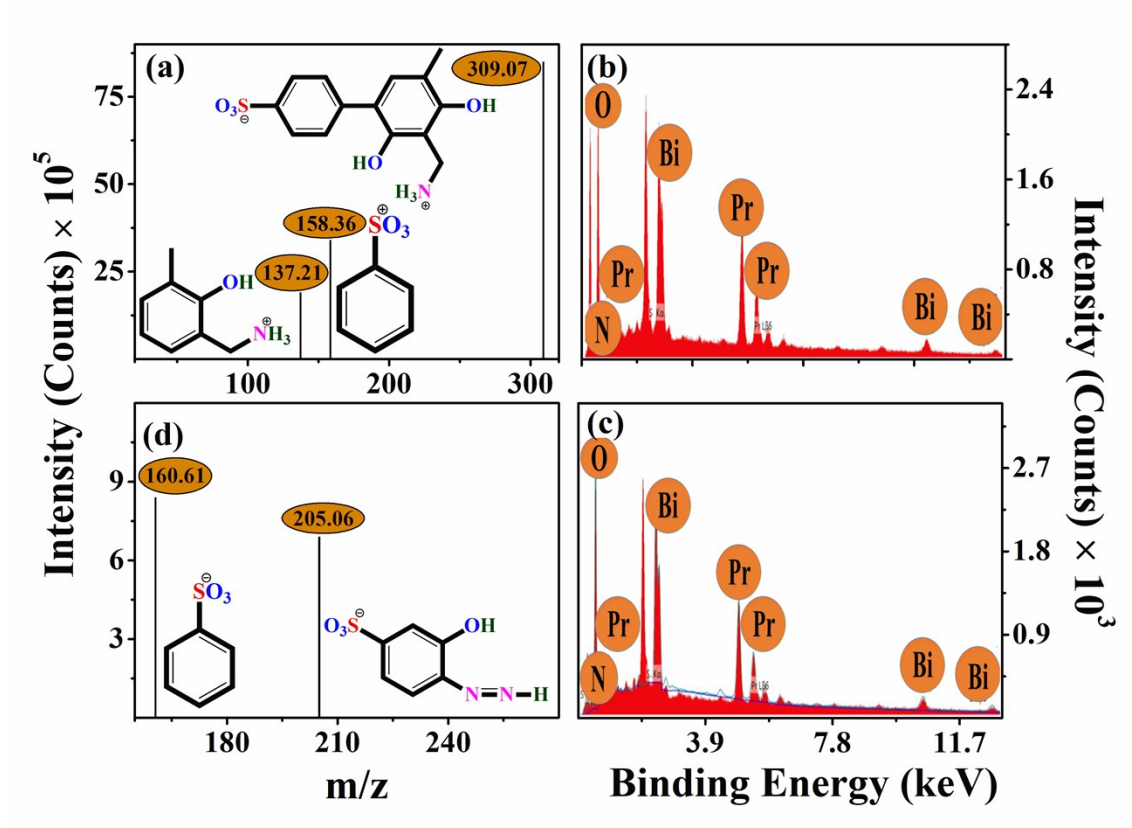

Fig. S4(a) and (b) show the mass spectrum of degraded products of XO dye employing $Pr_{0.60}Bi_{0.40}O_{2-\delta}$ as the catalyst and the EDS spectrum along with the elemental composition of the catalyst after its use. (c) and (d) show the mass spectrum of degraded products of MO dye employing $Pr_{0.60}Bi_{0.40}O_{2-\delta}$ as the catalyst and the EDS spectrum along with the elemental composition of the catalyst after its use.

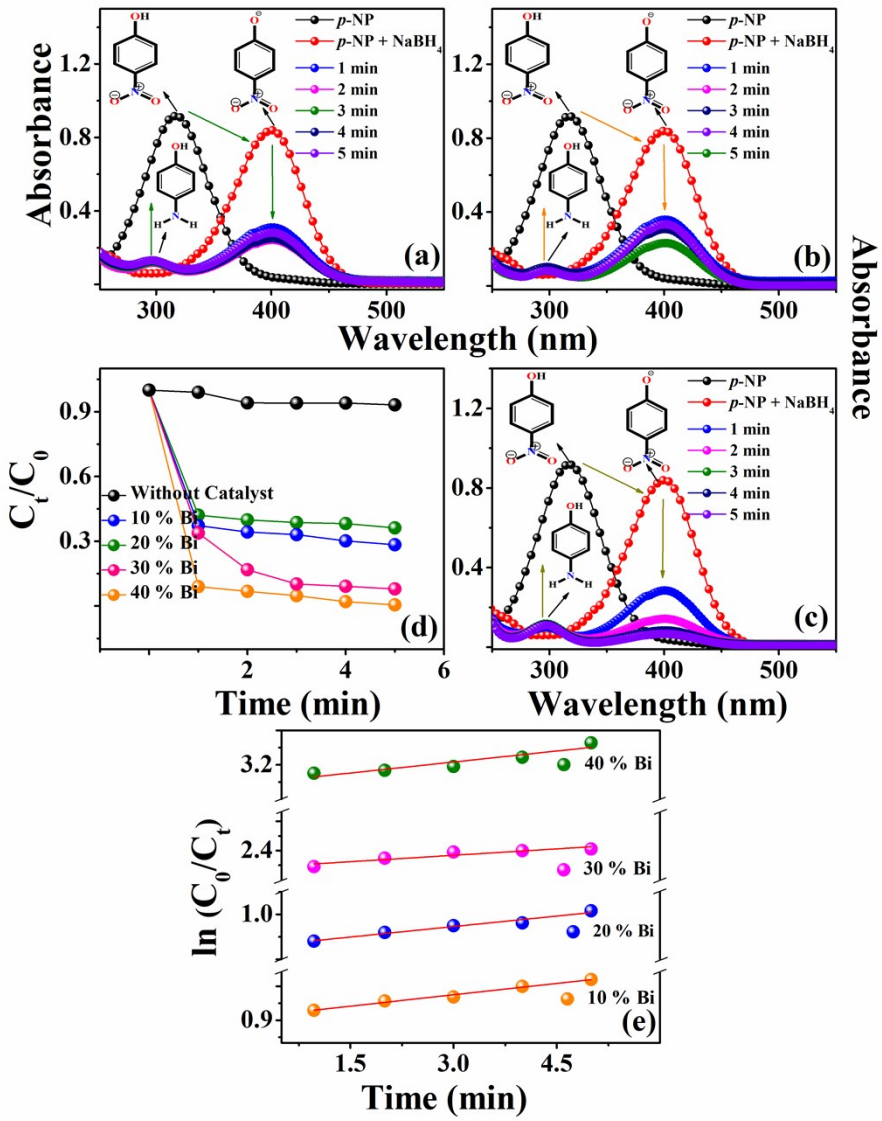

Fig. S5 shows time-dependent UV-visible spectra of *p*-NP in the presence of 4 mg of $NaBH_4$ and 20 mg of (a) $Pr_{0.90}Bi_{0.10}O_{2-\delta}$, (b) $Pr_{0.80}Bi_{0.20}O_{2-\delta}$ and (c) $Pr_{0.70}Bi_{0.30}O_{2-\delta}$ sample; (d) and (e) show the comparative plots of C_t/C_0 vs. time, ln C_0/C_t vs. time of reduction of *p*-NP using the samples $Pr_{1-x}Bi_xO_{2-\delta}$ (x = 0.10 - 0.40).

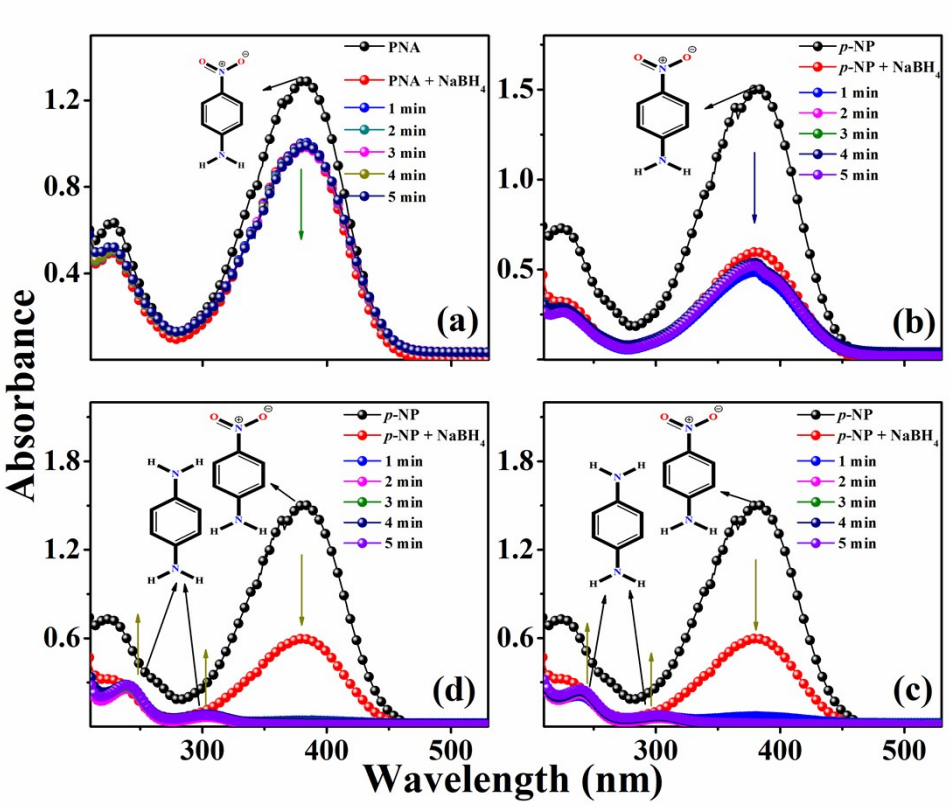

Fig. S6 shows time-dependent UV-visible spectra of *p*-NA in the presence of 4 mg of $NaBH_4$ and 20 mg of (a) $PrO_{1.83}$, (b) $Pr_{0.90}Bi_{0.10}O_{2-\delta}$, (c) $Pr_{0.80}Bi_{0.20}O_{2-\delta}$ and (d) $Pr_{0.70}Bi_{0.30}O_{2-\delta}$ sample.

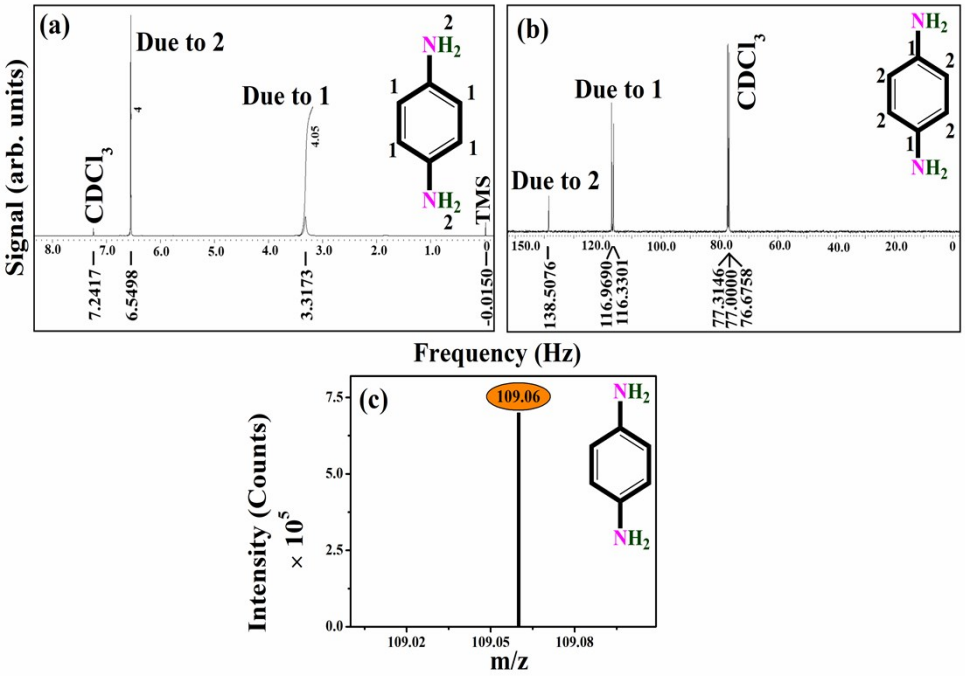

Fig. S7 shows (a) ^{1}H NMR, (b) ^{13}C NMR spectra, and (c) Mass spectral analysis of the recovered product from the reduction of *p*-NA.

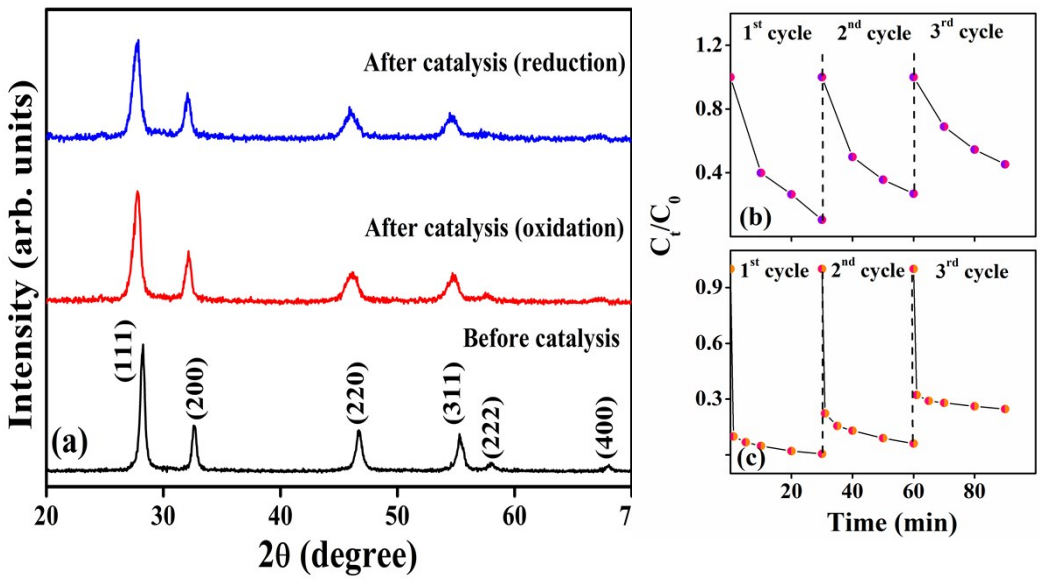

Fig. S8 (a) shows the PXRD pattern of the catalyst before and after its use for reduction and oxidation of *p*-NP and MO solutions, respectively. (b) and (c) show results from recyclability experiments employing $Pr_{0.60}Bi_{0.40}O_{2-\delta}$ as the catalyst for the oxidative degradation of MO (1×10^{-4} M) and reduction of *p*-NP (1×10^{-4} M) solutions, respectively.